INSTITUTE OF PHYSICS PUBLISHING JOURNAL OF MICROMECHANICS AND MICROENGINEERING

J. Micromech. Microeng. **14** (2004) 1064–1073 PII: S0960-1317(04)73833-4

Simulation studies on nonlinear dynamics and chaos in a MEMS cantilever control system

S Liu[1], A Davidson[2] and Q Lin[1]

[1] Department of Mechanical Engineering, Carnegie Mellon University, 5000 Forbes Ave., Pittsburgh, PA 15213, USA
[2] Department of Electrical and Computer Engineering, Carnegie Mellon University, 5000 Forbes Ave., Pittsburgh, PA 15213, USA

E-mail: artdav@ece.cmu.edu

Received 24 December 2003
Published 4 June 2004
Online at stacks.iop.org/JMM/14/1064
doi:10.1088/0960-1317/14/7/029

Abstract
We discovered period doubling and chaos in a simulated MEMS cantilever system with electrostatic sensing and actuation, intended for a MEMS based mass storage chip, with and without servo control. We used a graphical interface for a Poincaré map method that allowed us to simulate multiple initial conditions simultaneously. We investigated both the static and dynamic instabilities of the MEMS cantilever system subjected to weak and strong disturbances. We observed bistability and a Hopf bifurcation in the closed loop controlled cantilever system without disturbances. We simulated the loop gain and the phase margin when the system was subjected to weak disturbances. Furthermore, we have found the period doubling, chaos and strange attractors for both the open and closed loop cantilever systems subjected to strong disturbances. For one case the stable operation range is significantly reduced by 25% because of a chaotic response.

1. Introduction

Nonlinearities exist ubiquitously in microelectromechanical systems (MEMS). Examples include nonlinear spring and damping mechanisms [1, 2], nonlinear resistive, inductive and capacitive circuit elements [3, 4] and nonlinear surface, fluid, electric and magnetic forces [5–8]. In this work, we investigated nonlinearities in electrostatically actuated MEMS cantilevers. An open loop MEMS cantilever system with electrostatic actuation exhibits a snapping instability when the gap between two charged plates is decreased by one-third of its initial value. With servo control, this snapping instability can be made to occur at smaller plate separations, and hence the cantilever system can have a larger static stability range. Our work is focused on the stability of electrostatically actuated MEMS cantilevers both with and without servo control.

In 1890, Poincaré presented his geometrical interpretations of differential equations and the consequences of his results for celestial mechanics [9]. The Poincaré map, which is a stroboscopic view of the phase space, set Poincaré on the route to the discovery of dynamical chaos. Another investigation of chaotic behavior was reported in a seminal paper [10] by Lorenz, who proposed the Lorenz equations to model atmospheric dynamics and found the Lorenz attractor and fluid chaos. Chaos in nonlinear systems has become a major topic of study, and has also appeared in the general literature: one book on chaos [11] has been on *The New York Times* best-seller list.

Modeling, analysis and experimental results related to the nonlinear dynamic behavior of MEMS devices have been reported recently [1–8, 12]. Electrostatic and Casimir interactions can limit the range of positional stability of electrostatically actuated or capacitively coupled mechanical devices [7]. This stable range has been experimentally investigated by Buks and Roukes for a generic system consisting of a doubly clamped Au suspended beam, which is capacitively coupled to an adjacent stationary electrode. The data cannot be accounted for by simple theory; the discrepancy may be reflective of internal structural instabilities within the metal electrodes [7]. Global bifurcations involving snapping

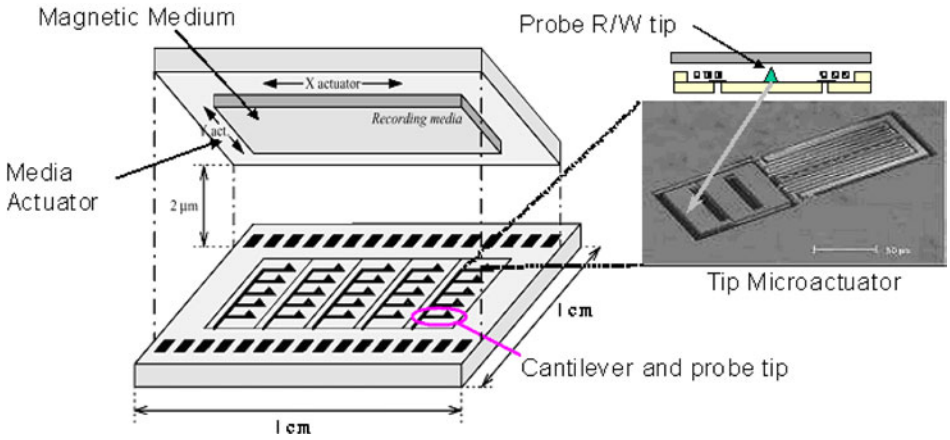

Figure 1. MEMS cantilevers used as tip actuators in a MEMS based probe storage chip.

instabilities of electrostatically actuated MEMS structures have been analyzed by Lu at Carnegie Mellon [5]. He addressed the snapping instability phenomenon with parallel-plate model based servoing, and observed an extended stable range of more than 67% of the initial gap [5]. Seeger and Boser used a negative capacitance to extend the stable range of a gap-closing actuator beyond voltage-controlled and the charge-controlled limits. They built a parallel-plate actuator that stably deflects more than 80% of the gap despite the presence of destabilizing parallel capacitance [13]. A second design of Seeger and Boser, in agreement with a two-degree-of-freedom model, was stabilized while tipping and has achieved a maximum deflection of 1.4 μm or 91% of the gap using less than 3 V [13]. Periodic and chaotic oscillations have been observed in an autonomous impact resonator by Bienstman *et al*. The experimental results have addressed such influences as the DC voltage, the charging and discharging resistors, the air damping, as well as the parasitic capacitance [4]. Theoretical analysis and experimental results on the dynamical behavior of a bistable MEMS oscillator have been published by Wang *et al*. They verified a model of a bistable MEMS devise using experimental data and they demonstrated the existence of a strange attractor in their MEMS device [6]. In this paper, we studied the nonlinear dynamics and chaos in a MEMS cantilever control system, which is based on Lu's electrostatically actuated MEMS cantilever system. Compared to the earlier works we discussed, we investigated the instability, nonlinear dynamics and chaos in the operating range for both open loop and closed loop controlled MEMS cantilever systems with snapping instability.

In our simulations the sources of nonlinearities in the MEMS cantilever system were the nonlinear electrostatic force and a separate nonlinear capacitive sensor. The Poincaré map method [14] was used as a tool for studying the stability of the cantilever system. Multiple initial conditions were considered simultaneously in our Poincaré map software. We investigated both the static and dynamic instability of the MEMS cantilever systems subjected to weak and strong disturbances. We found bistability and Hopf bifurcations in the closed loop controlled cantilever. We kept all the nonlinearities and observed the loop gain for the nonlinear control system. We used the Nyquist method to compute the phase margins of the MEMS control system under small disturbances. We also found significant chaotic regions in the excitation parameter space, and observed different strange attractors for both open and closed loop controls of the cantilever subjected to strong disturbances. This work is the first description of chaos in a MEMS cantilever system with an open-loop instability.

2. Background

2.1. Instability of the nonlinear MEMS cantilever

The MEMS cantilevers we modeled will be used in a MEMS based probe storage chip. As shown in figure 1, two chips produced with post-CMOS micromachining methods [5] are bonded together to form a MEMS based non-volatile magnetic mass storage device. The upper chip contains a moveable magnetic medium, which is addressed by an array of cantilevered probes illustrated on the bottom chip. Because of fabrication tolerances, a 2 to 3 μm gap is expected between the probe tips and the medium's surface after assembly. To read and write small marks, the tips must move to within a few nanometers of the medium, which in turn will require the cantilevers to move to within about 200 nm of the surface. This means that the cantilevers must have controlled actuation over 90% or so of the initial gap.

Our study is based on a real MEMS cantilever with dimensions of 4.5 μm $\times$ 80 μm $\times$ 200 μm [5]. As shown in figure 2, our MEMS cantilever is modeled as a nonlinear mass-spring-damper system with external electrostatic actuation, where mass $m = 3.5 \times 10^{-11}$ kg, spring constant $k = 0.17$ N m^{-1} and the damping coefficient $b = 1.78 \times 10^{-6}$ kg s^{-1}. The initial gap between the two parallel electrodes is $g = 3 \times 10^{-6}$ m. The normalized equation of the motion for the dynamic system is

$$\ddot{x} + \gamma \cdot \dot{x} + x = V_n^2 / (1 - x)^2 \qquad (1)$$

where $x = z/g$, $\gamma = b/\sqrt{mk}$, $\omega_0 = \sqrt{k/m}$ and $\tau = \omega_0 t$. Note that ω_0 is the cantilever's natural frequency, τ is the normalized time and $\dot{x}$ and $\ddot{x}$ are respectively the first- and second-order derivatives of x with respect to τ. The right-hand side of the equation represents the nonlinear electrostatic actuation force, where $V_n = V\sqrt{\varepsilon_0 A/2kg^3}$, and that V denotes the voltage applied across the electrode gap. The absolute dielectric constant of vacuum is $\varepsilon_0 = 8.854 \times 10^{-12}$ F m^{-1}, and the plate area is $A = 1.6 \times 10^{-9}$ m^2.

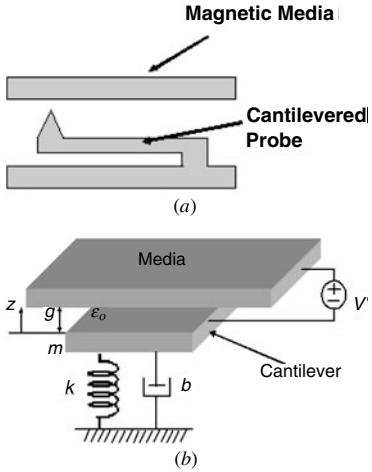

Figure 2. (*a*) Schematic picture of a MEMS cantilever. (*b*) The cantilever system modeled as a nonlinear single mass-spring-damper system with electrostatic actuation ($m = 3.5 \times 10^{-11}$ kg, $k =$ 0.17 N m^{-1}, $b = 1.78 \times 10^{-6}$ kg s^{-1} and the initial gap $g = 3$ μm).

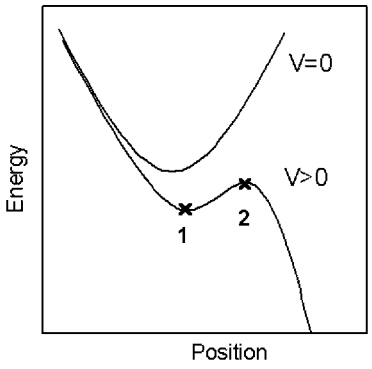

Figure 3. The cantilever system has a minimum energy position and a maximum energy position when a constant voltage is applied to the cantilever system. Snapping instability exists in this system.

The MEMS cantilever can be unstable because of the nonlinearities in electrostatic actuation. As schematically shown in figure 3, the electrostatic potential energy has a minimum and a maximum when a constant voltage is applied to the cantilever system. For a large enough voltage, the maximum disappears and the system becomes unstable. As a result, the cantilever plate snaps to the top plate; that is, a snapping instability occurs.

Stability has different characteristics for linear and nonlinear systems. For a linear control system, the loop gain, phase margin and gain margin can be obtained by standard methods. When the linear control systems are subjected to both weak and strong disturbances, we can use the linear theorems such as the loop gain and phase or gain margin to analyze stability. Linearization is traditionally used to analyze the stability of the nonlinear systems. However, some nonlinear behavior cannot be captured by the linearized systems. By keeping all the nonlinearities, we investigated both the stability and the nonlinear behavior of the nonlinear system. The nonlinear system can have multiple static operating points because of the multiple energy minima. The phenomena of bistability, multiple stability and Hopf bifurcation exist in the nonlinear system. Subjected to small disturbances, the system behaved almost like a linear system, allowing us to find the loop gain for this nonlinear system. Moreover, by keeping the nonlinearities in the system, we can obtain the Nyquist plot and phase or gain margin to analyze the system's stability. Under strong disturbances, the behavior of nonlinear control system can be hysteretic, chaotic or snapped closed. We used the Poincaré mapping method to investigate the nonlinear dynamics of the controlled cantilever under strong disturbances.

2.2. Poincaré maps and strange attractors

A Poincaré map is a sequence of points in phase space generated by the penetration of a continuous evolution trajectory through a generalized surface or plane in the space. For a periodically forced second-order nonlinear oscillator, a Poincaré map can be obtained by stroboscopically observing the position and velocity at a particular phase of the forcing function [14]. The Poincaré map method is an important tool in nonlinear dynamics, and can be used to distinguish between different states of motion such as periodic, quasiperiodic or chaotic orbits. As shown in table 1, a simple periodic response

Table 1. A Poincaré map is a stroboscopic view of phase space. A simple periodic response corresponds to a single-point attractor as in the top row. An unstable or chaotic response corresponds to a complex pattern of points, a strange attractor, shown in the bottom row. The middle row illustrates the phenomenon of period doubling.

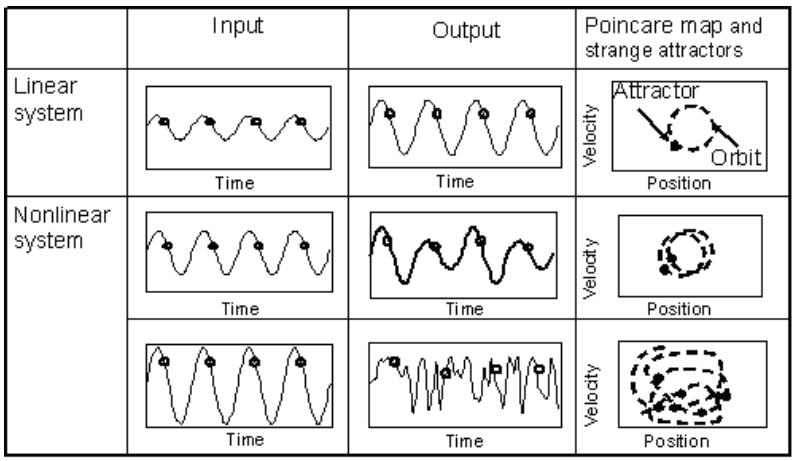

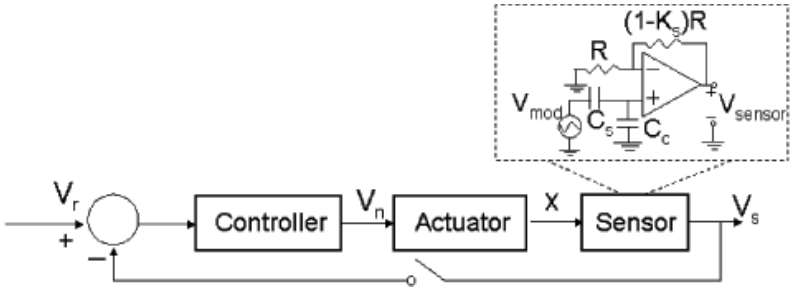

Figure 4. Open and closed loop controlled cantilever systems subjected to a disturbance. The inset is the schematic picture of the sensor.

in the linear system corresponds to a single-point attractor in a Poincaré map. Unstable or chaotic response in the nonlinear system corresponds to a complex pattern of points—a strange attractor that refers to the attracting set in phase space on which the chaotic orbits move. For the MEMS cantilever system subjected to strong disturbances, we observed such nonlinearites as the period doubling and chaos. So we used the Poincaré mapping method to investigate the nonlinear instability.

3. Open and closed loop controlled cantilever systems

The open loop cantilever system consists of the controller, the actuator plate and the sensor plate which is on the same cantilever as the actuator (figure 4). With a reference input voltage, an output voltage from the sensor can be obtained and translated to the displacement of the cantilever. When the sensor's output voltage is measured and the discrepancy between the reference input voltage and sensor's output voltage is sent to the controller, the cantilever system is under a closed loop control.

The actuation voltage applied between the cantilever plate and media plate is given by $V = G(V_{\text{ref}} - V_{\text{sensor}})$ in the closed loop system, where G is the controller gain, V_{ref} is the reference input voltage, and $V_{\text{sensor}} = K_s V_{\text{mod}} C_s/(C_c + C_s)$ is the sensor's amplifier output voltage. The sensor capacitance is $C_s = \varepsilon_0 A/(g(1-x)) - C_{s0}$, where $C_{s0} = \varepsilon_0 A/g$ is the initial sensor capacitance when normalized displacement $x = 0$ and C_c is the parasitic capacitance of the closed loop system. Note that we have subtracted the initial sense capacitance so that $C_s = 0$ when $x = 0$. In addition, K_s and V_{mod} are the gain and input of the sensor amplifier, respectively.

We use the following normalized equations for the sensor in our simulation:

$$\begin{cases} V_s = Kx/(h-x) \\ V_n = G(V_r - V_s) \end{cases} \tag{2}$$

where $V_r = V_{\text{ref}}\sqrt{\varepsilon_0 A/2kg^3}$ is the normalized reference input voltage. Here $d = C_c/C_{s0}$ is the ratio of the parasitic capacitance over the initial sensor capacitance, $h = d/(d-1)$ is a parameter affected by the parasitic capacitance and the initial sensor capacitance, and $K = K_s V_{\text{mod}}\sqrt{\varepsilon_0 A/2kg^3}\big/(d-1)$ is the normalized gain of the sensor amplifier. The normalized output voltage of the sensor and normalized voltage sent to the actuator plate are denoted as V_s and V_n, respectively. The simple sensor model described by equation (2), which is the same as case 1 in appendix, has been used in the simulation works on bistability, Hopf bifurcation, Nyquist plot and phase margin. For the real cantilever system, which has two sensor plates as shown in Lu's MEMS cantilever system (figure 1), the sensed displacements are the displacement of actuator plate times factor f_1 and factor f_2 separately. We use the more realistic model (case 2 in the appendix) in our other simulation works, such as snapping, period doubling, chaos and strange attractors. Under closed loop control (figure 4), the cantilever has a wider stable displacement range. We investigated the stability of both the open and closed loop controlled cantilever systems subjected to disturbances.

To study the nonlinear cantilever system, we developed a new Matlab-based simulation tool with graphical interface based on the Poincaré map method. This interface allows multiple initial conditions to be selected directly on the phase plane plot on the screen and tracked simultaneously as they flow toward attractors. A typical use of our Poincaré map simulation tool is shown in figure 5, where the simulation begins with a set of 36 initial conditions represented by the 36 dots. In practice, more or fewer initial conditions can be used depending on design needs. By simulating multiple trajectories simultaneously and plotting the results as Poincaré maps (figure 5(*b*)), we can quickly locate multiple attractors. Thus, our Poincaré mapping software can be used to study chaotic vibrations more efficiently and clearly than with other simulation tools. The nonlinear behavior of this cantilever system with and without closed-loop control was studied using this graphical interface and Poincaré mapping with normalized variables.

The accuracy of the model and the correctness of the Poincaré map simulation code were verified with experimental data in the static case. In figure 6, we plotted displacement versus reference voltage from an experimental cantilever, our dynamic simulations with full nonlinearity and a static theoretical calculation. We used parameters measured from the experimental system operating in the closed loop [5]. Although the experimental data are from a limited range, they fit our calculations without any adjustable parameters. Thus we are reasonably confident that our models captured the effect of nonlinearities in the system. In what follows, the simulation results in this paper are based on these verified nonlinear models and program code.

4. Bistability

We first study the static behavior of the closed loop. From equations (1) and (2) with $h = 1$, the state space representation

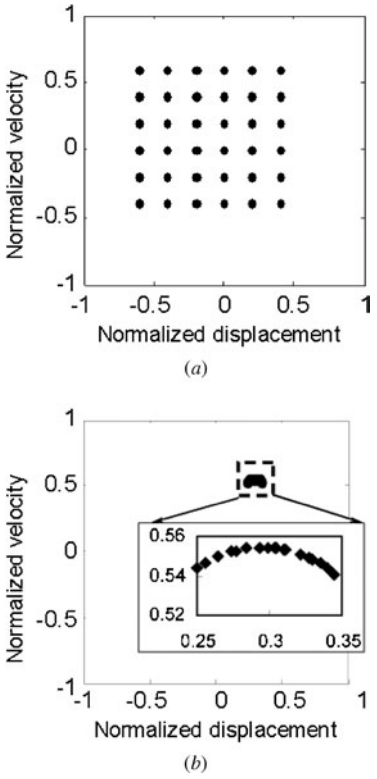

Figure 5. Nonlinear simulations are simultaneously performed with multiple initial conditions. For example, displayed in the graphical interface are (*a*) 36 initial conditions and (*b*) the corresponding Poincaré maps (with a close-up view). ($V_r = 0.35$, $a_n = 0.3704$, $\gamma = 0.7$, $\Omega = 1.0$, $K = 0.083$, $G = 2.4$, r is infinite.)

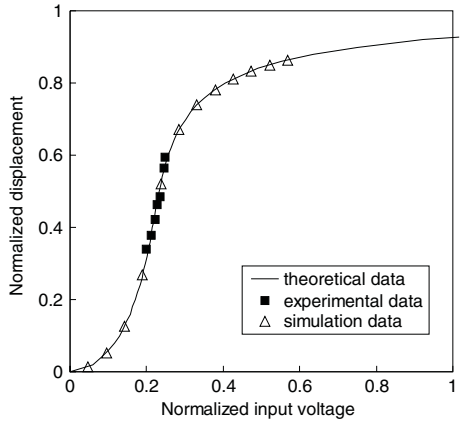

Figure 6. Static displacement versus reference voltage curves from experiment, static theory and dynamical simulation. The experimental data fits without any adjustable parameters, indicating that we have reasonable models for the nonlinearities ($g = 3.3$ μm, $\gamma = 0.7$, $h = 1.01$, $K = 0.083$, $G = 2.4$, $r = 10$).

of the closed loop controlled cantilever system is given by the following normalized equations:

$$\begin{cases} \dot{x} = y \\ \dot{y} = -\gamma y - x + \frac{G^2(V_r - V_s)^2}{(1-x)^2} \\ \dot{V}_s = -r\left(V_s - \frac{Kx}{1-x}\right) \end{cases} \tag{3}$$

where r is the bandwidth of the low pass filter placed after the sensor in the closed loop system. Note that $h = 1$ corresponds to $C_c \gg C_{s0}$, which means that the parasitic capacitance is much larger than the initial sensor capacitance.

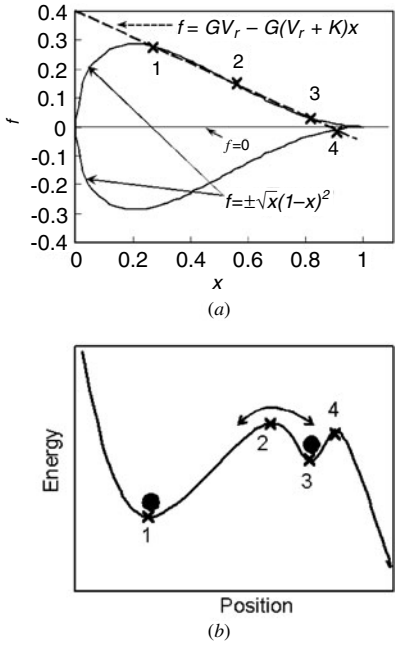

Figure 7. Four equilibrium positions can be found, which indicates that the control cantilever system could be bistable. (*a*) The graphical solutions of the equilibrium positions: $x_1 = 0.283$, $x_2 = 0.565$, $x_3 = 0.775$, $x_4 = 0.895$, $K = 0.06$, $G = 1.0$ and $V_r = 0.405$. (*b*) Schematic picture of the potential energy with four equilibrium positions.

The equilibrium state of the system can be obtained by setting all time derivatives to zero ($\dot{x} = \dot{y} = \dot{V}_s = 0$) in the above equations. From equations (3) we can write the total force F on the cantilever in the closed loop, normalized, as

$$F = -x + \frac{G^2(V_r(1-x) - Kx)^2}{(1-x)^4} \tag{4}$$

The resulting equilibrium condition is written such that the total force is zero as

$$\pm\sqrt{x}(1-x)^2 = GV_r - G(V_r + K)x. \tag{5}$$

The solutions of the equilibrium positions are obtained graphically by plotting the left- and right-hand sides of equation (5) as functions of x. By varying the system parameters, we can find up to four equilibrium positions, as shown in figure 7(*a*). For example, when $K = 0.06$, $G = 1.0$ and $V_r = 0.405$, the four equilibrium positions are $x_1 = 0.283$, $x_2 = 0.565$, $x_3 = 0.775$, $x_4 = 0.895$. These equilibria correspond up to two minima and two maxima of the potential energy in the system, as shown in figure 7(*b*). In the case that the cantilever system is bistable, two energy minima exist and the system can be stable in two positions.

The fact that the closed loop system can be bistable has been verified by results from dynamic simulation. As shown in figure 8, the gain has been reduced ($G = 1.0$, $K = 0.06$), and the displacement versus reference voltage has become hysteretic, indicating bistability in the closed loop. This bistability is expected from the form of the total force on the cantilever in the closed loop from equation (4). For $G = 1.0$, $K = 0.06$, and the fact that F has four real zeros, bistability occurs for a

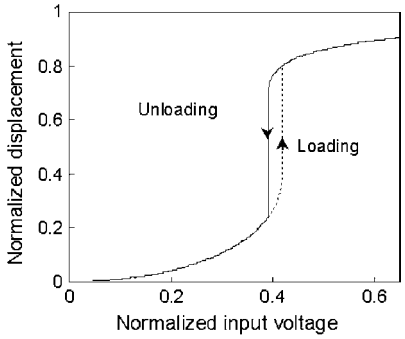

Figure 8. Bistability of the controlled cantilever system with a smaller control gain, using dynamic simulation ($\gamma = 0.7$, $K = 0.06$, $G = 1.0$, r is infinite.).

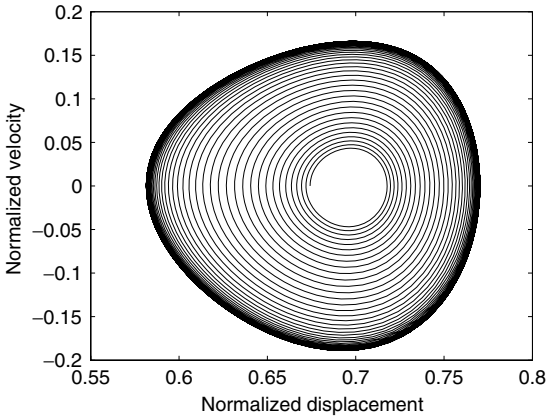

Figure 9. Hopf bifurcation is observed in the MEMS closed loop controlled cantilever system with the parameters of $G = 1.6$; $K = 0.0835$, $\gamma = 0.7$, $r = 10$, $V_r = 0.35$, disturbance $a = 0$, initial condition (0.674, 0, 0.173).

range of x before the cantilever snaps close at $x > 0.9$. Note that the singularity at $x = 1$ is of the fourth order.

5. Hopf bifurcation

As parameters are changed in a nonlinear system, the stability of the equilibrium points changes as well as the number of the equilibrium points, which is studied as the subject of bifurcation theory. A Hopf bifurcation is the emergence of a limit cycle oscillation from an equilibrium state as some system parameter is varied [14].

In the nonlinear closed loop controlled cantilever system, we observed the Hopf bifurcation in the simulation. As shown in figure 9, when the parameters prescribed are $G = 1.6$, $K = 0.0835$, $\gamma = 0.7$, $r = 10$, the cantilever is at rest initially with a displacement of $x = 0.674$ when the input reference voltage is $V_r = 0.34$. As an input voltage V_r is increased to 0.35, the system becomes dynamically unstable. As the motion amplifies, nonlinearities come into effect and the motion is bounded within a limit cycle, which represents the Hopf bifurcation. Furthermore, we investigated the range of the Hopf bifurcation when the bandwidth of the low pass filter is changed. The results in figure 10 show that both the critical input voltage to the range of Hopf bifurcation and the one to the range of snapping are increased when

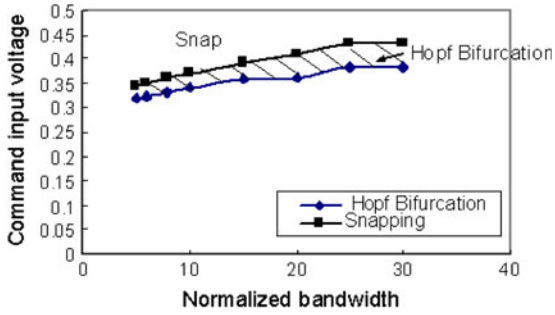

Figure 10. The range of Hopf bifurcation is increased when the bandwidth of the low pass filter is increased ($G = 1.6$; $K = 0.0835$, $\gamma = 0.7$, initial condition (0, 0, 0)).

the bandwidth of the low pass filter is increased ($G = 1.6$; $K = 0.0835$, $\gamma = 0.7$, initial condition (0, 0, 0)). When the Hopf bifurcation is observed in the system, the system will snap with either increasing input voltage or decreasing bandwidth of the low pass filter. The Hopf bifurcation is caused by the nonlinearities in the system and is the well-known scenario for chaotic vibration. In our MEMS cantilever systems, the Hopf bifurcation is one characteristic precursor to the snapping. In linear systems there is no limit cycle; thus snapping has essentially no warning.

6. Instability of the cantilever system subjected to a small sinusoidal disturbance

In sections 6 and 7, we have investigated the dynamic stability of the cantilever system subjected to both weak and strong disturbances. So the state space representation of the closed loop controlled cantilever system subjected to disturbances is given by the following normalized equations:

$$\begin{cases} \dot{x} = y \\ \dot{y} = -\gamma y - x + \frac{G^2(V_r - V_s)^2}{(1-x)^2} + a_n \cos(\Omega\tau) \\ \dot{V}_s = -r\left(V_s - \frac{Kx}{1-x}\right) \end{cases} \tag{6}$$

where, $a_n = a/\left(\omega_0^2 g\right)$, $\Omega = \omega/\omega_0$, a and ω are the disturbance magnitude and frequency, ω_0 is the cantilever's natural frequency, τ is the normalized time as in equation (1).

6.1. Loop gain for nonlinear systems

For a closed loop nonlinear control system subjected to a small displacement or force disturbance, we obtained the loop gain while keeping the nonlinearities within the system [16].

Although many physical relationships are represented by linear equations, a careful study of physical systems reveals that even the so-called 'linear systems' are really linear only in limited operating ranges. Systems may be operated near an equilibrium point, and the input signals may be considered as small perturbations to the equilibrium. There are also exceptions to this common scenario. For some systems such as an on–off controlled system, nonlinearities are present for signals of any magnitude [15]. However, for most of the general systems, which operate in the vicinity of an equilibrium point for small signals, we can approximate the nonlinear system by a linear one. Such a linear system is

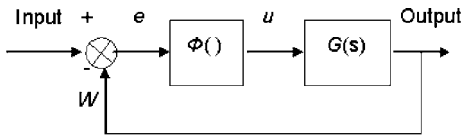

Figure 11. The 'standard' nonlinear control system configuration consists of a linear dynamic plant having the transfer function $G(s)$ and a nonlinear element.

an approximation to the nonlinear system considered within a limited operating range.

The 'standard' nonlinear control system configuration consists of a linear dynamic plant having the transfer function $G(s)$ and a nonlinear element as shown in figure 11 [17]. The nonlinear characteristic is designated by

$$u = \phi(e). \tag{7}$$

We considered the standard nonlinear control system in figure 11, where the nonlinear element takes the form of a variable gain. For some values of the variable gain, the gain margin or phase margin will go to zero and the system will oscillate.

In our simulation, we kept all the nonlinearities in the nonlinear system. We injected a small sinusoidal disturbance as an input to the closed loop nonlinear systems and traced the path of the signal around the loop. Keeping all the nonlinearities and the loop closed, we defined the open loop gain as

$$\text{Loop gain} = \lim_{\text{input}\to 0} \frac{\Delta w}{\Delta e}. \tag{8}$$

As shown in figure 12, we injected a small sinusoidal displacement or force disturbance into the closed loop controlled cantilever system to obtain the loop gain. Because the displacement disturbance and the force disturbance are in the same branch of the closed loop system, the same loop gain is obtained (figure 13).

6.2. Nyquist plot and phase margin

To investigate the dynamic stability, the cantilever system is subjected only to a small sinusoidal force disturbance (figure 12), with magnitude (a_n) much less than the magnitude of the electrostatic force. Using our simulation on the closed loop controlled cantilever system with equation (8), we obtained the open loop gain of the system subjected to a force disturbance in the loop. When the normalized bandwidth of the low pass filter (r) is 10, the Nyquist plot of the loop gain is shown in figure 13.

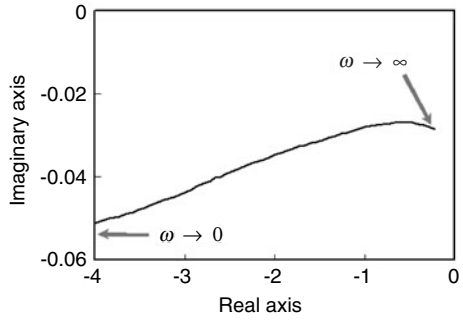

Figure 13. Nyquist plot of the loop gains measured from a force disturbance in the controlled cantilever system when the normalized bandwidth of the low fast filter is 10 ($r = 10, x = 0.64, \gamma = 0.7, K = 0.083, G = 2.4, a_n = 0.001$).

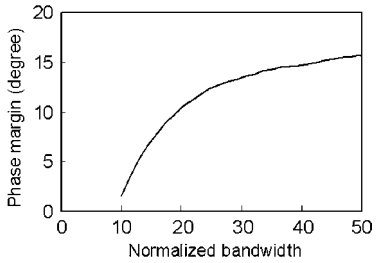

Figure 14. Phase margin obtained from the loop gains in the controlled cantilever system ($x = 0.64, \gamma = 0.7, K = 0.083, G = 2.4, a_n = 0.001$).

From the Nyquist plot, we calculated the phase margin (figure 14). The phase margin approaches zero as the bandwidth of the low pass filter decreases. The cantilever system becomes unstable when the phase margin is negative. Therefore, for very small disturbances, the Nyquist criteria are still valid, and the controlled cantilever system will be stable with enough bandwidth in the control loop. However, large disturbances will push the system out of the linear regime, and the Nyquist stability criteria no longer apply and a nonlinear analysis method, such as Poincaré mapping, is needed.

7. Instability of the cantilever system subjected to a strong sinusoidal disturbance

7.1. Snapping with strong disturbances

The system is subjected to a sinusoidal disturbance with input frequency prescribed as the same as the cantilever's natural frequency and with magnitudes (a_n) slowly increased from zero to a value large enough to generate a nonlinear response.

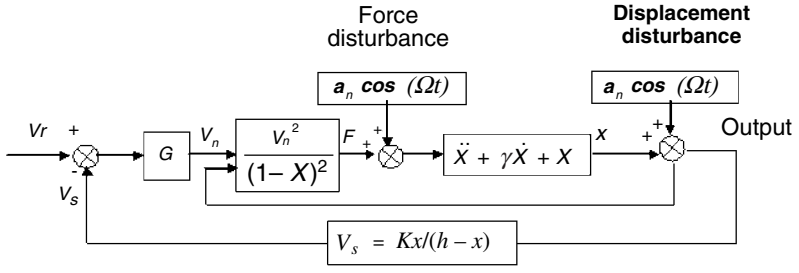

Figure 12. Diagram of the closed loop controlled cantilever system subjected to different disturbances.

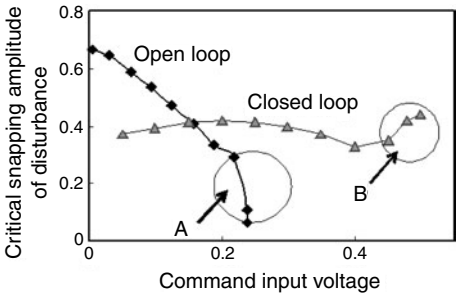

Figure 15. Critical snapping disturbance amplitude for open and closed loop systems ($\gamma = 0.7$, $\Omega = 1.0$, $K = 0.083$, $G = 2.4$, r is infinite).

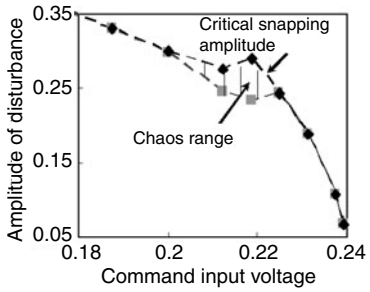

Figure 16. Chaos range of disturbance amplitude for the open loop system at different reference voltages (region A in figure 15).

Snapping occurs as a_n reaches a critical value a_{nc}, which is plotted as a function of the reference voltage V_r in figure 15 for both the open and closed loop systems. It can be seen that a_{nc} decreases with increasing V_r for the open loop system, and is nearly constant under closed loop control. For the open loop system, when the reference voltage V_r is increased, the position of the cantilever is close to the snapping point. So the magnitude of the disturbance which the system can resist is decreased. The closed loop controlled system, on the other hand, has a high immunity to the disturbances for high reference voltage V_r. Compared with the open loop system, the closed loop controlled system can achieve a wider stable operating range and is less sensitive to higher disturbances at the operating points for large displacements.

7.2. Period doubling, chaos and strange attractors

In our nonlinear MEMS cantilever dynamical system, there are some characteristic precursors to the snapping, such as the period doubling and chaos. In conducting any of these tests for period doubling phenomenon or chaotic vibrations, we varied one or more of the control parameters in the system. In our simulation, we varied the amplitude of the disturbance. We further used Poincaré mapping to explore V_r and a_n values corresponding to the circles A and B in figure 15. Interestingly, period doubling and chaos are observed with disturbance amplitudes that are smaller than a_{nc}. For both open and closed loop systems, the chaotic range of a_n values can be significant (as large as 25% of a_{nc}), as shown as a function of V_r in figures 16 and 17. From these results, we know that the nonlinear MEMS cantilever system is not always stable before snapping. The behavior of period doubling and chaos, which can be significant and not explored by linearized systems, exists for some range of the parameter space. In some

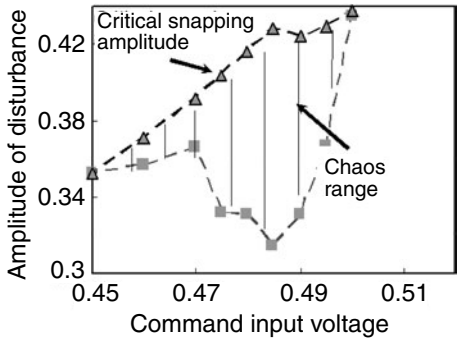

Figure 17. Chaos range of disturbance amplitude for the closed loop system at different reference voltages (region B in figure 15).

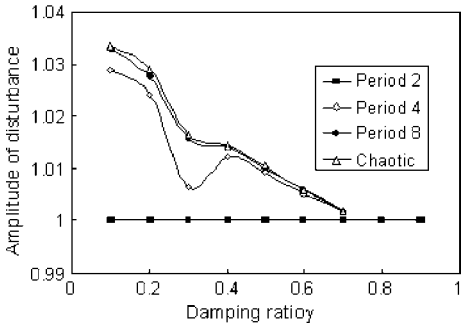

Figure 18. Phenomena of period doubling by normalizing to the period 2 transition are apparent for cantilever systems with different damping ratios. The nonlinear cantilever system with a smaller damping ratio is more unstable and has a larger area of period doubling and chaos ($\Omega = 1.0$, $K = 0.083$, $G = 2.4$, r is infinite).

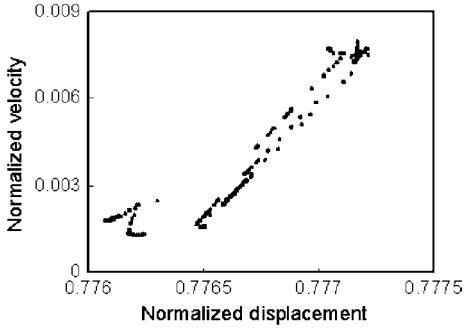

Figure 19. A strange attractor which occupies a small region of phase space has been found more easily than alternative methods in the closed loop system with $V_r = 0.48$, $a_n = 0.3502$, $\gamma = 0.7$, $\Omega = 1.0$, $K = 0.083$, $G = 2.4$, and r is infinite.

applications, such as our cantilever system, we want to avoid these unstable ranges.

Furthermore, we investigated period doubling of the cantilever system with a different damping ratio in our simulation. As shown in figure 18, period doubling ranges by normalizing to the period doubling range of period 2, transitions are apparent for cantilever systems with different damping ratios. The results show that the nonlinear cantilever system with a smaller damping ratio is more unstable and has a larger area of period doubling and chaos.

There are many different strange attractors within the chaotic area, depending on the disturbance amplitude. Figure 19 shows a strange attractor (as observed in figure 15,

Table 2. Sensor models used in our simulation work.

Sensor	Equations of capacitor sensor	Normalized equations	Used in
Case 1	$\begin{cases} C_s = \varepsilon_0 A/(g(1-x)) - C_{s0} \\ V_{\text{sensor}} = K_s V_{\text{mod}} C_s/(C_c + C_s) \\ V = G(V_{\text{ref}} - V_{\text{sensor}}) \end{cases}$	$\begin{cases} V_s = Kx/(h-x) \\ V_n = G(V_r - V_s) \end{cases}$	$\begin{cases} \text{Bistability} \\ \text{Hopf bifurcation} \\ \text{Nyquist plot, phase margin} \end{cases}$
Case 2	$\begin{cases} C_{s1} = \varepsilon_0 A/(g(1-123x/183)) - C_s 0 \\ C_{s2} = \varepsilon_0 A/(g(1-153x/183)) - C_s 0 \\ C_s = C_{s1} - C_{s2} \\ V_{\text{sensor}} = K_s V_{\text{mod}} C_s/(C_c + C_s) \\ V = G(V_{\text{ref}} - V_{\text{sensor}}) \end{cases}$	$\begin{cases} C_{s1} = \varepsilon_0 A/(g(1-123x/183)) - C_s 0 \\ C_{s2} = \varepsilon_0 A/(g(1-153x/183)) - C_s 0 \\ C_s = C_{s1} - C_{s2} \\ V_{\text{sensor}} = K_s V_{\text{mod}} C_s/(C_c + C_s) \\ V_n = G(V_r - V_{\text{sensor}}\sqrt{\varepsilon_0 A/2kg^3}) \end{cases}$	$\begin{cases} \text{Snapping} \\ \text{Period doubling} \\ \text{Chaos and strange attractor} \end{cases}$
	$C_{s0} = \varepsilon_0 A/g$, $V_r = V_{\text{ref}}\sqrt{\varepsilon_0 A/2kg^3}$, $h = d/(d-1) \approx 1$, $d = C_c/C_{s0}$		
	$K = K_s V_{\text{mod}}\sqrt{\varepsilon_0 A/2kg^3}/(d-1)$, C_c is the parasitic capacitance		

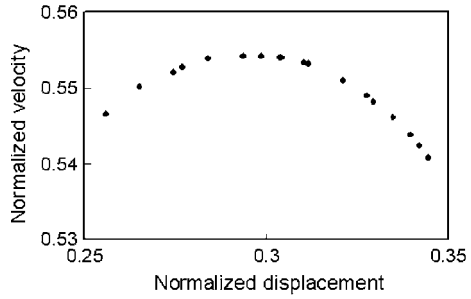

Figure 20. Another strange attractor of chaos which occupies a notably larger range of the phase space has been observed for the controlled cantilever system with $V_r = 0.35$, $a_n = 0.3704$, $\gamma = 0.697$, $\Omega = 1.0$, $K = 0.083$, $G = 2.4$, and r is infinite.

region B), which occupies a small region of phase space, and so would be difficult to find by alternative methods. In figure 20, another strange attractor that we observed in the closed loop system occupies a much wider region of the phase space. By observing the strange attractors in the Poincaré map, we know that the system is in chaotic vibration. In the parameter space, different initial conditions for the nonlinear dynamical system will cause different vibrations, such as the stable periodic motions or chaotic motions. Our graphical interface with the Poincaré map method allows multiple initial conditions to be selected directly on the phase plane plot on the screen. Multiple trajectories can be simulated simultaneously; thus, chaotic vibrations and multiple strange attractors can be found more easily than with other simulation tools.

8. Conclusions

We have developed and used simulation methods to investigate both the static and dynamic instability of the MEMS cantilever system subjected to weak and strong disturbances. We have verified bistability in the closed loop controlled cantilever system in both theoretical analyses and our simulation with full nonlinearities. We have observed the Hopf bifurcation, a characteristic precursor to the snapping, in the closed loop controlled cantilever system applied with reference input voltage without any disturbance. We have analyzed the loop gain and phase margin for nonlinear control systems. The Nyquist criteria are shown to be valid for the MEMS control system under small disturbances, which can be stable with high enough bandwidth in the feedback loop. For an electrostatically actuated MEMS cantilever subjected to strong disturbances, we used the Poincaré map with a graphical interface for selecting multiple initial conditions. We were able to easily find significant chaos in the response of realistic models. For the nonlinear MEMS cantilever system, we have observed period doubling, chaos and strange attractors for both the open loop system and the closed loop system. For one case the stable operation range of the closed loop system is significantly reduced by 25% because of a chaotic response.

Our future work will include research on reducing the order of the closed loop force polynomial, which would eliminate the bistable behavior, and improve overall stability as the gap approaches zero. A potential alternative pull-away design will be investigated to reduce the order of singularity at $x = 1$.

Acknowledgments

The authors are grateful to Drs M S-C Lu and G K Fedder at Carnegie Mellon for their help in the experiment. We verified some of our results with 'Dynamics Solver,' (http://tp.lc.ehu.es/jma/ds/ds.html) free software written by Juan Aguirregabiria of the University of the Basque Country, Spain. We thank Parker Lin of Carnegie Mellon for a critical reading of the manuscript. This research is supported in part by the Pittsburgh Digital Greenhouse (contract number 101230-PDG) and NASA (contract number NAG8-1799).

Appendix

Two different sensor models are used in our simulation work (table 2). (1) Case 1 is the simple model in which the sensor displacement is the same as the displacement of actuator plate. The simple sensor model has been used in the simulation works on bistability, Hopf bifurcation, Nyquist plot and phase margin. (2) For the real cantilever system, which has two sensor plates as Lu's MEMS cantilever system (figure 1), the sensed displacements are the displacement of actuator plate times f_1 and f_2 separately. We use this more realistic model (case 2) in our other simulation works, such as snapping, period doubling, chaos and strange attractors.

References

[1] Carley L R, Bain J A, Fedder G K, Greve D W, Guillou D F, Lu M S-C, Mukherjee T and Santhanam S 2000 Single-chip computers with microelectromechanical systems-based magnetic memory *J. Appl. Phys.* **87** 6680–5

[2] Adams S G, Bertsch F and MacDonald N C 1996 Independent tuning of the linear and nonlinear stiffness coefficients of a micromechanical device *Proc. 9th IEEE Int. Workshop on Micro Structures, Sensors, Actuators, Machines and Systems (MEMS '96)* pp 32–37

[3] Tan K K, Lee T H and Zhou H X 2001 Micro-positioning of linear piezoelectric motors based on a learning nonlinear PID controller *IEEE/ASME Trans. Mechatron.* **6** 428–36

[4] Bienstman J, Puers R and Vandewalle J 1998 Periodic and chaotic behaviors of the autonomous impact resonator *Proc. 11th IEEE Int. Workshop (MEMS 98)* pp 562–567

[5] Lu M S-C 2002 Parallel-plate micro servo for probe-based data storage *PhD Dissertation* Dept. of Electrical and Computer Engineering, Carnegie Mellon University, Pittsburgh, PA.

[6] Wang Y C, Adams S G, Thorp J S, MacDonald N C, Hartwell P and Bertsch F 1998 Chaos in MEMS, parameter estimation and its potential application *IEEE Trans. Circuits Syst.* I **45** 1013–20

[7] Buks E and Roukes M 2001 Metastability and the Casimir effect in micromechanical systems *Europhys. Lett.* **54** 220–6

[8] Lee Y-K, Deval J, Tabeling P and Ho C-M 2001 Chaotic mixing in electrokinetically and pressure driven micro flows MEMS 2001 *the 14th IEEE Int. Conf.: Micro Electro Mechanical Systems* pp 483–86

[9] Petersen I 1993 *Newton's Clock, Chaos in the Solar System* (New York: Freeman) chapter 7

[10] Lorenz E N 1963 Deterministic nonperiodic flow *J. Atmos. Sci.* **20** 130–41

[11] Gleick J 1987 *Chaos: Making a New Science* (New York: Viking Press)

[12] Burdess J S 1999 Modelling of nonlinearities in MEMS devices *IEE Seminar on Microengineering, Modelling and Design* p 42

[13] Seeger J I and Boser B E 2003 Negative capacitance for control of gap-closing electrostatic actuators *TRANSDUCERS '03, The 12th Int. Conf. on Solid State Sensors Actuators and Microsystems (Boston, June)* pp 484–7

[14] Moon F C 1987 *Chaotic Vibrations: An Introduction for Applied Scientists and Engineers* (New York: Wiley)

[15] Ogata K 1997 *Modern Control Engineering* (Upper Saddle River, NJ: Prentice Hall) 3rd edn p 58

[16] Middlebrook R D 1975 Measurement of loop gain in feedback systems *Int. J. Electron.* **38** 485–512

[17] Friedland B 1996 *Advanced Control system design* (Englewood Cliffs, NJ: Prentice Hall) pp 58–61